

Simulation and Optimization of Integrated Air-Conditioning and Ventilation Systems

Christopher R. Laughman, Hongtao Qiao, Scott A. Bortoff, Daniel J. Burns
Mitsubishi Electric Research Laboratories, Cambridge, MA, USA
{laughman,qiao,bortoff,burns}@merl.com

Abstract

One promising path for reducing the power consumption and improving the performance of building HVAC systems involves the coordinated design and operation of individual subsystems. This objective requires careful consideration of the dynamic interactions between the subsystems serving the occupied spaces. We propose a physical model-based approach for evaluating, optimizing, and designing control algorithms for integrated collections of subsystems to achieve high overall system performance. This approach is used in this paper to optimize the setpoints of and design dynamic controllers for an overall HVAC system consisting of a dedicated outdoor air system (DOAS) and a variable refrigerant flow (VRF) system serving a large occupied space. By optimizing the system inputs, we demonstrate that the energy consumption can be reduced by 15% as compared to the system with non-optimized inputs, and that non-intuitive system dynamics can be managed through systematic control analysis and design.

Introduction

Variable refrigerant flow (VRF) systems are becoming popular for residential and commercial HVAC applications due to a number of features that differentiate them from conventional variable air volume (VAV) systems. Among these features are their ease of installation, the reduced building volume required because of the absence of air ductwork, their high part load efficiency due to variable speed compressors and fans, and their high energy efficiency via heat recovery which enables simultaneous heating and cooling (Aynur, 2010).

Unfortunately, standard VRF system architectures are often not integrated with a means of providing fresh-air ventilation. Indoor air quality (IAQ) guidelines that specify ventilation air requirements, such as ASHRAE Standard 62.1 (ASHRAE, 2016), must therefore be satisfied by incorporating additional ventilation systems into the building's overall HVAC system. 100% outdoor air systems such as dedicated outdoor air systems (DOAS) are often used to meet these IAQ requirements, as they separately condition the outdoor air to reduce the latent loads on the space and provide a means for distributing and verifying the supply of fresh air to occupied spaces in an energy-efficient manner (Mumma and Shank,

2001). The overall HVAC system architecture, which thus consists of parallel VRF and DOAS subsystems, thus provides both space conditioning and ventilation by separately managing the latent and sensible loads. Because the building spaces effectively couple the behavior of both the DOAS and VRF subsystems, control and operation strategies that are designed to operate each subsystem independently can result in poor building-level performance. For example, the coupled interactions between subsystems make it difficult to select control inputs for each subsystem that minimizes the system-level energy consumption. Conventional decoupled control architectures, such as using subsystems to independently regulate the supply air temperature and the room air temperature, also do not allow for the independent control of humidity in the occupied space. The operation of the subsystems thus must be jointly coordinated to account for their dynamic coupling to achieve high system-level performance.

A variety of different approaches to integrating DOAS and VRF systems have been explored in recent literature. Kim et al. (2016) used a genetic algorithm to identify a set of optimal setpoints for a set of polynomial equipment models of an integrated HVAC system in heating mode, and was able to reduce energy consumption for the overall system by approximately 20%. Zhu et al. (2015) also developed strategies for controlling the operation of an integrated HVAC system by using polynomial models of both systems to identify an optimal supply air setpoint temperature, which improved the energy efficiency of the overall system by 12% in the summer and 3% in the winter. In comparison, Rane et al. (2016) combined a VRF system with a DOAS system that employed indirect evaporative cooling and liquid desiccant dehumidification to increase the COP of the overall system for a given design condition by 40%.

While these results are encouraging, careful study of this prior work reveals a few important limitations. Perhaps the most important of these is the emphasis on steady-state models for the integrated HVAC system; while proper consideration of a steady-state design condition is important, a well-designed system response to changes in the load and the operating conditions is essential to the reliable operation of a practical integrated system. In addition, all of the above methods also rely upon polynomial equipment

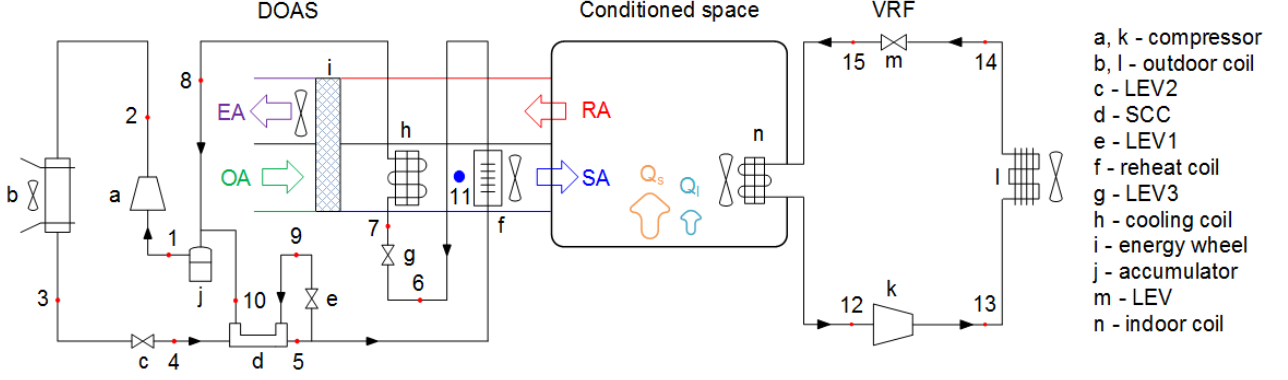


Figure 1: The architecture for an HVAC system that integrates both VRF and DOAS subsystems.

models, which are not suitable for extrapolation over the wide range of possible equipment conditions.

Recent advances in modeling and simulation technology have facilitated the creation of dynamic physics-based white-box models of HVAC systems and equipment, which have much improved extrapolative abilities over traditional black-box methods. Modelica (2014), a declarative, object-oriented, and open physical modeling language, is particularly amenable to describing the dynamics of thermofluid systems such as are found in HVAC systems (Wetter et al., 2016). Component models can thus be created and interconnected to simulate and analyze large-scale system dynamics.

In this work, we develop a set of dynamic physics-based Modelica models for the VRF and DOAS systems, and couple them to an model of an occupied room from the Modelica Buildings Library (Wetter et al., 2014) for the purpose of designing a control architecture that maintains the room temperature, humidity, and ventilation rate at user-specified setpoints. Figure 1 illustrates such an overall HVAC system architecture. Moreover, the energy consumption of the integrated system is also minimized via the use of optimized setpoints, which are determined by the use of a separate set of steady-state models for the VRF and DOAS systems that are formulated in C#; such distinct models were used because the identification of steady-state operating points using dynamic models requires extremely long simulation times, rendering the prospect of optimization impractical.

In Section 2 of this paper, we describe the steady-state and dynamic heat exchanger models, which exhibit important differences though they are based on a common one-dimensional fluid flow model. Other component models for both the DOAS and VRF systems, such as for the compressors, expansion valves, and room, are then described in Section 3. We then use these component models in Section 4 to construct models of the DOAS system and a prototype VRF system with a single evaporator, and demonstrate the energy savings that may be attained by jointly optimizing all control inputs for an building-level HVAC system which integrates the two subsystems. A con-

trol architecture for the integrated system which has good transient performance is then described in Section 5, demonstrating the efficacy of this approach.

Heat exchanger models

The heat exchangers lie at the core of the system models, not only because they mediate the heat transfer between the indoor and ambient spaces, but also because they dominate the temporal response of the systems over the time scales of interest for the dynamic models. One particularly important characteristic of these models is their consistency; since the outputs of the setpoint optimization from the steady-state models will be used as inputs to the dynamic models, the models must be verified to be equivalent in some sense. Both the steady-state and dynamic models of the heat exchangers used in this work were thus based upon the assumption of one-dimensional fluid flow, in which the properties only vary in the direction of the flow, and are averaged over every cross section of the pipe.

A variety of other assumptions were employed to simplify the models. These included 1) the fluid is Newtonian, 2) negligible axial heat conduction in the direction of the fluid flow, 3) negligible viscous dissipation, 4) negligible contribution to the energy equation from the potential and kinetic energy of the refrigerant, 5) dynamic pressure waves are negligible in the momentum equation, and 6) the liquid and vapor are in thermodynamic equilibrium in each volume in the two-phase region.

In consideration of these assumptions, the basic equations of fluid flow expressing the mass, momentum, and energy conservation in the heat exchangers underlying both the steady-state and dynamic models can be expressed as:

$$\frac{\partial(\rho A)}{\partial t} + \frac{\partial(\rho A v)}{\partial x} = 0 \quad (1)$$

$$\frac{\partial(\rho v A)}{\partial t} + \frac{\partial(\rho v^2 A)}{\partial x} = -A \frac{\partial P}{\partial x} - F_f \quad (2)$$

$$\frac{\partial(\rho u A)}{\partial t} + \frac{\partial(\rho v h A)}{\partial x} = v A \frac{\partial P}{\partial x} + v F_f + \frac{\partial Q}{\partial x}, \quad (3)$$

where ρ is the density, A is the cross-sectional area of the flow, v is the velocity, P is the pressure, F_f is the

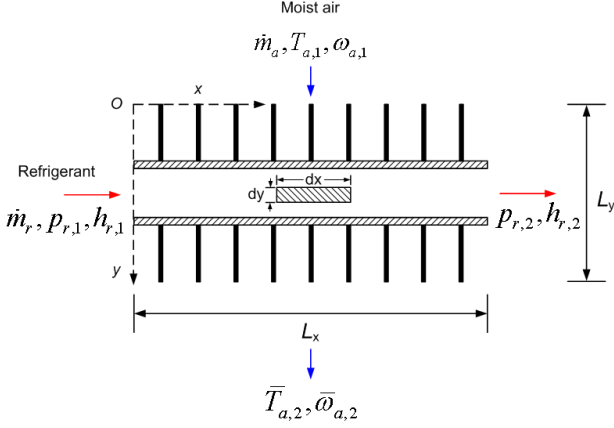


Figure 2: Picture of the control volume for the air-to-refrigerant heat exchanger.

frictional pressure drop, u is the specific internal energy, h is the specific enthalpy, and Q is the heat flow rate into or out of the fluid. These equations describe the fluid flow in an Eulerian reference frame for all heat exchanger models used in this research, and can be adapted to a finite control volume discretization of the refrigerant pipe by using the Reynolds transport theorem. Further adaptations corresponding to the particular type of heat exchanger model under consideration (e.g., steady-state or dynamic, fin-tube or coaxial) are discussed in the corresponding subsections.

Steady-state models

The steady-state tube-fin heat exchanger model is based on an approach which evaluates the performance of each tube separately, with its associated refrigerant and air-side parameters. Simulation starts with the refrigerant inlet tube of a given circuit, and progresses sequentially through each of the following tubes until the outlet is reached. When the surface temperature is above the dew point of the air stream, only sensible heat transfer occurs on the air side. In contrast, simultaneous heat and mass transfer occurs on the external surfaces of the heat exchanger when the surface temperature is below the dew point, resulting in removal of water vapor from the air stream via condensation.

The mass and momentum balances for each control volume for this steady-state model represent a straightforward modification of the underlying balance equations provided in (1)-(3). Mass conservation is enforced by assuming that the mass flow rates into and out of each control volume are identical and constant. The momentum balance is enforced by using an empirical correlation to characterize the pressure drop between cells as a function of the mass flow rate \dot{m} , e.g.,

$$\Delta P = K \frac{(\Delta P)_0}{\dot{m}_0^2} \dot{m}^2, \quad (4)$$

where the nominal values of K , $(\Delta P)_0$, and \dot{m}_0 were determined by using the Colebrook correlation for the

single-phase friction factor and the Friedel correlation for two-phase multipliers (Stephan, 2010).

The steady-state tube-fin heat exchanger model distinguishes between three regimes of operation: fully dry, fully wet, and partially wet. In the fully dry case, heat transport between the refrigerant and the air is driven by the temperature difference, and water vapor in the moist air stays in the gaseous phase. The heat transfer process between the air and refrigerant in a cross-flow configuration with one tube, as shown in Figure 2 can be described by

$$\dot{m}_a \frac{dx}{L_x} c_{p,a} T_a = -U_o (T_a - T_r) dA_o \quad (5)$$

$$\dot{m}_r dh_r = -\dot{m}_a c_{p,a} \frac{dx}{L_x} [T_a(x, L_y) - T_a(x, 0)] \quad (6)$$

where T is the fluid temperature, $c_{p,a}$ is the specific heat capacity of the air, and the overall heat transfer coefficient, based on the total external surface area, is defined as $U_o = 1/(R_{ad} + R_{md} + R_r)$. The thermal resistances are calculated based on AHRI Standard 410 (AHRI, 2001). Under the additional assumption that the air inlet temperature is uniform, the one-dimensional refrigerant temperature distribution and two-dimensional air temperature distribution can be obtained by integrating (5) and (6). The heat transfer rate of the tube can be readily computed once the refrigerant and air temperatures have been obtained. In the fully wet case, all of the surface temperatures are below the dew point of the air stream. The simultaneous heat and mass transfer between the moist air and the refrigerant can thus be described by

$$\frac{T_w - T_r}{R_{mW} + \zeta R_r} = \frac{T_a - T_w}{R_{aW}} + \alpha_m (\omega_a - \omega_w) (h_{g,a,w} - h_{f,w}) \quad (7)$$

$$\frac{T_w - T_r}{R_{mW} + \zeta R_r} dA_o = -\frac{\dot{m}_a}{L_x} (dh_o - h_{f,w} d\omega) \quad (8)$$

$$\dot{m}_r dh_r = -\frac{\dot{m}_a}{L_x} \left[h_a(x, L_y) - h_a(x, 0) - \int_{y=0}^{y=L_y} h_{f,w} d\omega \right] \quad (9)$$

$$d\dot{m}_w = -\frac{\dot{m}_a}{L_x} dx d\omega \quad (10)$$

$$d\dot{m}_w = \alpha_m (\omega_a - \omega_w) dA_o. \quad (11)$$

where α is the mass transfer rate, ζ is the fin effectiveness, and ω represents the humidity ratio of the moist air. In the partially wet case, part of the coil is dry because the surface temperature is above the entering air dew-point temperature, while the remainder of the coil is wet with the surface temperatures below the entering air dew-point temperature. Because the performance of the dry and wet portions of the coil are evaluated separately, the boundary between the these regions must be determined by using numerical iterations which equate the coil surface temperatures

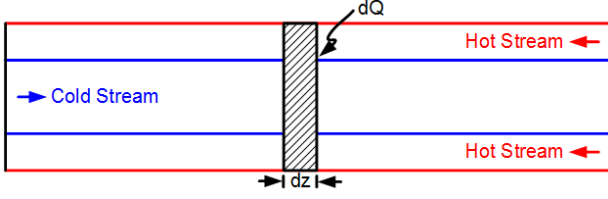


Figure 3: Picture of the control volume for the coaxial heat exchanger.

with the air dew point temperature, since these temperatures are equal on the dry-wet boundary. More information about these steady-state models for the tube-fin heat exchangers can be found in Qiao and Laughman (2016).

In comparison to the tube-fin models, the coaxial heat exchanger is a refrigerant-to refrigerant heat exchanger in a counterflow configuration, as illustrated in Figure 3. This device is used to improve the system performance by increasing the subcooling of liquid refrigerant leaving the condenser to prevent flash gas formation at the inlet of the expansion device. The inlet conditions of both primary and secondary streams can be either two-phase or subcooled liquid, depending on the operating conditions. Models of this type of heat exchanger can be quite complex because of the challenges inherent in tracking the phase transition point when phase changes occur in both streams. A zone-by-zone model was developed in this work, in which the exact location of the phase change can be computed in either stream, to avoid an expensive finite volume formulation.

An energy balance over a differential segment of this heat exchanger yields a simple expression for the heat balance, e.g.,

$$dQ = U(T_h - T_c)dA = -\dot{m}_h dh_h = \dot{m}_c dh_c. \quad (12)$$

The effectiveness-NTU method is used to obtain the heat transfer between both streams if they are both in the single-phase region. When one stream is two-phase and the other is single-phase, the two-phase saturated refrigerant temperature is assumed to vary linearly with the tube length, allowing (12) to be rewritten as

$$\begin{aligned} dQ &= (\dot{m}c_p T)_{1ph} \\ &= U [T_{sat,out} + (T_{sat,in} - T_{sat,out})z - T_{1ph}] dA. \end{aligned} \quad (13)$$

When both streams are in the two-phase region, the heat transfer rate can readily be computed as

$$Q = UA(T_{h,in} + T_{h,out} - T_{c,in} - T_{c,out})/2. \quad (14)$$

In these models, the possibility of phase change for each stream is determined by comparing the possible heat transfer rate between the two streams under the assumption of phase change allowed by the second law of thermodynamics to the required heat transfer rate for phase change to occur. If the possible heat

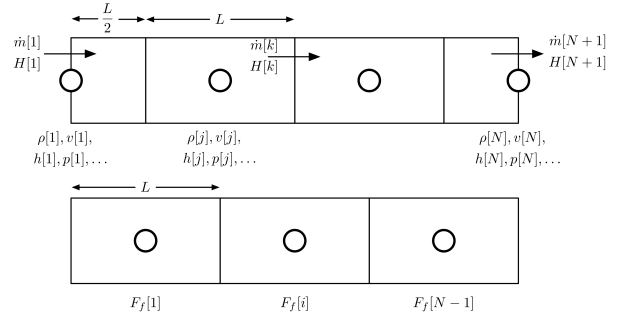


Figure 4: Staggered discretization grid used to model the dynamics of the fluid.

transfer rate is larger than the required heat transfer rate, then phase change occurs in one or both streams; otherwise, no phase change occurs in either stream. Numerical iterations are used to compute the location of phase change such that the specific enthalpy of the refrigerant at the transition point is equal to the saturated liquid or vapor enthalpy corresponding to the local refrigerant pressure. These models were written in C# to utilize a thermodynamic property library developed at the University of Maryland (Aute and Rademacher, 2014).

Dynamic models

The set of partial differential equations ((1)- (3)) describing the fluid flow through the refrigerant pipe were discretized to form a set of ordinary differential equations (ODEs) for the dynamic heat exchanger models. A staggered flow grid (Patankar, 1980), illustrated in Figure (4), was used to eliminate pressure variations caused by numerical artifacts, while the size of the set of ODEs was dictated by the number of control volumes used to subdivide the pipe's length. This resulted in the following set of equations, which use different indices for each conservation equation depending on the particular grid of relevance.

$$\frac{d(\rho_j V_j)}{dt} = \dot{m}_k - \dot{m}_{k+1} \quad (15)$$

$$\begin{aligned} \frac{d(\dot{m}_i)}{dt} l &= \rho_j v_j^2 A_j - \rho_{j+1} v_{j+1}^2 A_{j+1} + \\ &\quad \frac{A_j + A_{j+1}}{2} (P_{j+1} - P_j) + F_{f,i} \end{aligned} \quad (16)$$

$$\begin{aligned} \frac{\partial(\rho_j u_j A_j)}{\partial t} &= H_k - H_{k+1} + \\ &\quad v_j A_j (P_{j+1} - P_j) + v F_{f,i} + Q_j. \end{aligned} \quad (17)$$

In these equations, the i indices refer to the momentum grid, the j indices refer to the thermal grid, and the $k = j + 1$ indices refer to the boundaries of the thermal grid for each volume V_j . In addition, the term H_k is defined as

$$H_k = \dot{m}_k \bar{h}_{upstream,j}, \quad (18)$$

and the mixed-cup specific enthalpy \bar{h} is equal to the *in situ* specific enthalpy under the homogeneous flow assumption (Laughman et al., 2015).

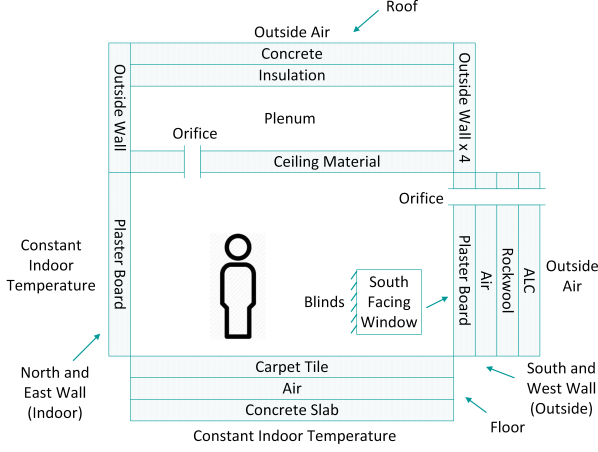


Figure 5: Diagram of simulated room construction.

Thermodynamic property equations also play an important role in these mathematical models. By specifying the pressure P and mixture specific enthalpy h as the state variables for the equations of fluid motion, these property relations determine the relations between the intensive and extensive properties for a volume of fluid in thermodynamic equilibrium and allow the calculation of any other properties in the thermodynamic phase space, such as temperature, density, or specific internal energy from the state variables. Using this parameterization, the derivatives of the refrigerant mass $M(P, h)$ and total internal energy $U(P, h)$ in each finite volume from (15) and (17) can be written as

$$\frac{dM}{dt} = V \left(\left. \frac{\partial \rho}{\partial P} \right|_h \frac{dP}{dt} + \left. \frac{\partial \rho}{\partial h} \right|_P \frac{dh}{dt} \right) \quad (19)$$

$$\frac{dU}{dt} = V \left[\left(h \left. \frac{\partial \rho}{\partial P} \right|_h - 1 \right) \frac{dP}{dt} + \left(\left. \frac{\partial \rho}{\partial h} \right|_P h + \rho \right) \frac{dh}{dt} \right] \quad (20)$$

Component Models

A number of other component models were needed to create a full dynamic cycle models including both the DOAS and VRF systems integrated with an occupied space. These component models included those of the compressor, expansion valve, energy recovery wheel, and occupied room with its associated thermal and airflow dynamics. Because the heat exchanger dynamics generally dominate those of the vapor compression cycle over the timescales of minutes to hours, static models of the compressor and expansion devices are commonly used in these models as they are simpler than dynamic models and do not increase the numerical stiffness of the system of ODEs. An additional benefit of these static models, particularly relevant to this work, was that exactly the same static component model formulations could be used in both the steady-state and dynamic models, thereby improving the correspondence between these two model types.

Variable-speed high-side scroll compressors, in which the motor is cooled by the compressed high-pressure

discharge refrigerant, were used in this work. These static compressor models are characterized by a performance map of curve-fitted equations describing their steady-state operation over a wide range of saturated suction and discharge temperatures. The volumetric efficiency map for the compressor as a function of the suction pressure P_{suc} , discharge pressure P_{dis} , and compressor frequency f is given by

$$\eta_v = c_0 + c_1 \varphi + c_2 \varphi^2 + c_3 \varphi^3 + c_4 (P_{dis} - P_{suc})(1 + c_5 P_{suc}), \quad (21)$$

where $\varphi = P_{dis}/P_{suc}$, $c_i = a_{i,1} + a_{i,2}\bar{\theta} + a_{i,3}\bar{\theta}^2$, and $\bar{\theta} = f/f_{nom}$. Similarly, the power \dot{W} consumed by the compressor is determined by:

$$\dot{W} = z_1 P_{suc} \dot{V}_{suc} (\varphi^{z_2} - z_3) + z_4, \quad (22)$$

where $z_i = b_{i,1} + b_{i,2}\bar{\theta} + b_{i,3}\bar{\theta}^2$. The coefficients $a_{i,j}$ and $b_{i,j}$ are fit from experimental data obtained for the system under consideration.

Electronic expansion valves are used in both subsystems. The mass flow rate through the throttle is determined by the flow coefficient, the flow area, the inlet density, and the pressure difference across the valve according to a standard orifice-type flow equation

$$\dot{m} = C_v a_v \sqrt{\rho_{in} \Delta P}, \quad (23)$$

where the flow coefficient C_v can be determined by regression using experimental data and the flow area a_v is specified by the user.

Similar algebraic fan models specified by standard fan laws (ASHRAE, 2008) were also used to describe the relationship between fan speed, volumetric flow rate of air through the fan, and the fan power consumption. These laws were scaled by nominal values of the fan speed, flow rate, and power collected from experimental data. In addition, we assumed that the building was kept at a constant pressure, so that the supply air flow rate and the exhaust air flow rate in the conditioned space are equal.

While a set of partial differential heat and mass transfer equations must be solved to construct a detailed dynamic model of the energy wheel, we simplified our analysis by assuming that the energy wheel has constant efficiencies for heat and mass transfer. The amount of sensible heat transfer and the amount of water vapor exchange between the outdoor air stream and the exhaust air stream can thus be determined by

$$\dot{q}_s = \eta_s \min(\dot{m}_{OACp,a}, \dot{m}_{RACp,a})(T_{OA} - T_{RA}) \quad (24)$$

$$\dot{m}_w = \eta_w \min(\dot{m}_{OA}, \dot{m}_{RA})(\omega_{OA} - \omega_{RA}). \quad (25)$$

One distinct advantage of the open Modelica language is that the wide array of publicly-available models created by the larger Modelica community can be easily modified and incorporated into projects, thereby leveraging the domain expertise of other

Parameter	Value
Room area (m ²)	828.4
Room height (m)	2.6
Plenum height (m)	1.3
Concrete slab thickness (m)	0.2
Window size (m ²)	44.52
Building location	San Francisco

Table 1: Room model parameters.

model authors as well as reducing the cost of model development. The performance of the overall integrated system was evaluated by using the dynamic DOAS and VRF cycles as well as the the dynamic room model from the LBNL Modelica Buildings Library (Wetter et al., 2014), which uses a fully-mixed air model and uses a detailed characterization of the various heat gains and thermal performance of the building envelope. A schematic of the conditioned space can be seen in Figure 5, while the most pertinent parameters are provided in Table 1.

Two other simpler room models were used to test and evaluate the performance of the optimized cycle models. For simplicity, the steady-state models used a lumped adiabatic approximation for the room, so that the sensible and latent cooling capacities of both the VRF and DOAS systems was constrained to be equal to the sensible and latent cooling loads in the space. A dynamic lumped adiabatic room model was also used to compare the power consumption of the steady-state and dynamic models, as the use of different room models for the steady-state and dynamic models would result in very different results.

System solution and optimization

This collection of component models was first used to construct steady-state and dynamic integrated system models, which were employed in turn by an optimization method to determine the setpoints that result in energy-optimal steady-state operation. Accordingly, this section first discusses the process by which the component models were used to construct and solve the system models, introduces the formulation of the optimization problem and the methods used to solve it, and then presents the results from three different use cases to demonstrate the efficacy of this optimization method.

System solution

While the construction of the dynamic cycle models via the interconnection of component models was facilitated by Modelica’s object-oriented paradigm, the traditional imperative programming-based architecture of the steady-state models necessitated a careful treatment of the system solution process. A steady-state models for the DOAS was constructed from the component models illustrated in Figure 1, while an provisional single-evaporator VRF system, also displayed in the same figure, was constructed by using the same models of the compressor, expansion valve,

and evaporating and condensing heat exchangers as were used in the DOAS to ensure that the cooling capacities of both systems were approximately matched. These steady-state component models are solved using a method similar to that of the enthalpy marching solver (Winkler et al., 2008), in which the thermodynamic state at each junction is determined by propagating the specific enthalpy around the cycle in the order of the refrigerant flow, beginning at the junction connected to the compressor suction. The boundary conditions of the heat exchangers are the refrigerant mass flow rate, inlet pressure, and inlet enthalpy, whereas the boundary conditions for the flow control components (e.g., compressors and valves) are the inlet pressure, inlet enthalpy, and outlet pressure. This results in a set of unknown variables \mathbf{x} and residual equations \mathbf{r} for the DOAS that consist of

$$\mathbf{x}_D = [p_1, p_2, p_4, p_5, p_7, p_9, h_1, h_5, \dot{m}_{LEV1}, T_{11}, \phi_{11}]^T \quad (26)$$

$$\begin{aligned} \mathbf{r}_D = & [p_8 - p_1, p_{10} - p_1, \dot{m}_c - \dot{m}_{LEV2}, \\ & \frac{\dot{m}_{LEV1}h_{10} + \dot{m}_{LEV3}h_8}{\dot{m}_{LEV1} + \dot{m}_{LEV3}} - h_1, \\ & h_{SCC,po} - h_5, P_{SCC,po} - P_5, T_{11} - T_{a,eo}, \\ & \phi_{11} - \phi_{a,eo}, \Delta SH_{SCC} - \Delta SH_{SCC,set}, \\ & \Delta SH_e - \Delta SH_{e,set}, \Delta SC - \Delta SC_{set}]^T, \end{aligned} \quad (27)$$

where SH denotes evaporator superheat, and SC denotes condenser subcooling. In comparison, the set of unknown variables and residual equations for the VRF system consists of

$$\mathbf{x}_V = [p_{12}, p_{13}, p_{15}, h_{12}]^T \quad (28)$$

$$\begin{aligned} \mathbf{r}_V = & [p_{eo} - p_{12}, h_{eo} - h_{12}, \\ & \Delta SH - \Delta SH_{set}, \Delta SC - \Delta SC_{set}]^T. \end{aligned} \quad (29)$$

Note that this proposed formulation implicitly constrains the expansion valve positions for each of the cycles through the specification of an evaporator (or subcooling coil) superheat setpoint, as well as the amount of refrigerant mass in each cycle through the specification of a value for a condenser subcooling setpoint. These constraints must therefore also be satisfied in the dynamic models through the use of feedback to regulate the evaporator superheat and the careful specification of the initial conditions to achieve the desired refrigerant mass in the cycle.

Equations (27) and (29) are solved for each individual system via the Newton-Raphson method to predict its performance given a specified set of ambient conditions, fan speeds and compressor frequencies. The metrics used to assess performance include the overall capacity, power consumption, and air temperatures. As the sensible and latent thermal loads are specified when evaluating the performance of the integrated system, the compressor frequencies of the DOAS f_D and the VRF system f_V are added to the concatenated vector of unknowns $\mathbf{x}_t = [\mathbf{x}_D \ \mathbf{x}_V]^T$ that are

determined during the solution process, and the following residual equations

$$\begin{bmatrix} r_{c,D} \\ r_{c,V} \end{bmatrix} = \begin{bmatrix} Q_{sens,D} + Q_{sens,V} - Q_{sens,set} \\ Q_{lat,D} + Q_{lat,V} - Q_{lat,set} \end{bmatrix} \quad (30)$$

are added to the concatenated residual vector $\mathbf{r}_t = [\mathbf{r}_D \ \mathbf{r}_V]^T$.

Optimization

The problem formulation used to minimize the overall power consumption \dot{W}_t of the integrated system while delivering the required capacity to the conditioned space, as described at the end of the previous subsection, is given by

$$\begin{aligned} &\text{minimize} && \dot{W}_t(\dot{V}_{OA,D}, \dot{V}_{OA,V}, \dot{V}_{supply}) \\ &\text{subject to} && \dot{V}_{min} \leq \dot{V}_{supply} \leq \dot{V}_{max}. \end{aligned} \quad (31)$$

The design variables for this formulation are the outdoor flow rates for each of the individual subsystems as well as the supply air flow rate for the DOAS. This inequality constraint indicates that the supply air flow rate \dot{V}_{supply} is bounded between minimum (\dot{V}_{min}) and maximum (\dot{V}_{max}) values, which may be obtained from such standards as ASHRAE 62.1.

The compressor speeds and the indoor unit fan speed for the VRF system are not listed among the set of design variables for the optimized system because they are implicitly constrained by performance variables. In particular, the compressor speeds are constrained by space loads, the valve positions are constrained by specifying the steady-state evaporator superheat for both systems to be equal to a setpoint (2 °C), and the VRF indoor unit fan speed was fixed at a nominal value under the assumption that this variable would remain under user control.

This constrained optimization problem was converted into an unconstrained problem by incorporating the bounds on the volumetric air flow rate via the transformation given by the volumetric air flow rate according to

$$\dot{V}_{supply} = \dot{V}_{min} + (\dot{V}_{max} - \dot{V}_{min}) \sin^2 y_{supply} \quad (32)$$

where the new optimization variable y_{supply} is unconstrained. We used the nonlinear conjugate gradient method developed by Fletcher and Reeves (1964) to solve this unconstrained minimization problem, due to its well-proven performance. A minor adaptation was made to this method by using a quadratic interpolation method to avoid numerical computation of the partial derivatives when determining the optimal step length in the search direction.

Results

We studied the behavior of these models and optimization methods in a number of different computational experiments to evaluate their performance. These models were first calibrated to experimental data to ensure their validity, after which they were

Parameter	Value	Parameter	Value
T_{room} (°C)	25	ϕ_{room} (%)	50
$T_{SC,D}$ (°C)	15	$T_{SC,V}$ (°C)	10
$T_{SH,D}$ (°C)	2	$T_{SH,V}$ (°C)	2
SCC $T_{SH,D}$ (°C)	2	$\dot{V}_{IA,V}$ (CFM)	2400

Table 2: Constant parameters for the three test cases.

used to study the potential reduction in energy performance accompanying the use of the optimized input setpoints. In addition, the dynamic models were also simulated with the same optimal setpoints to assess the consistency of the model outputs for the steady-state and dynamic formulations in preparation for their use in designing control architectures for the integrated HVAC system.

While the physics-based structure of these models generally improves their extrapolative capabilities, it was still necessary to calibrate them to experimental data to ensure that the model output was representative of a realizable system. Detailed measurements over a range of conditions were thus collected from an experimental DOAS system to characterize its behavior, and we adjusted a set of tuning parameters in the models (e.g., heat transfer coefficients, compressor maps) so that the output variables of the simulation matched the experimental data. This calibration step was carried out on both a component basis as well as a system basis to assure model validity at both scales. While a detailed analysis of this model calibration step is beyond the scope of this paper, the refrigerant pressures and temperatures, as well as air-side cooling capacity, all matched the experimental data with errors of less than 10%.

Our approach to reducing the energy consumption of an integrated system through optimized setpoints was tested on three main use cases: a baseline case, one case with hotter ambient conditions, and one case in which the building occupancy increases from 50 to 70 people. In each of these cases, the energy consumption of the system with optimized setpoints is compared to the energy consumption of the system which also meets the performance requirements but uses fan speeds from the middle of their respective operating ranges. Many of the process operating points and conditions, provided in Table 2, are chosen to be constant across all three test cases for consistency.

Results from these computational experiments, as shown in Table (3), suggest that substantial improvements in energy efficiency may be attained through the use of optimized setpoints. The nominal conditions of Case 1, with ambient temperature $T_{amb} = 35$ °C and relative humidity $\phi_{amb} = 80\%$, suggest that the energy consumption of the integrated system can be reduced by 21.9% over a nominal choice of fan speeds, while the hotter outdoor conditions of Case 2 indicate even greater energy savings of nearly 28%. In comparison, the scenario of Case 3 in which the building has 20 additional occupants shows an improve-

ment of 11.7%, as the nominal fan speeds chosen are closer to the optimized fan speeds. While the use of occupancy-scheduled ventilation of 17 CFM of fresh air/person as per ASHRAE 62.1 results in a significant reduction of the supply air flow rate, this model-based approach indicates that the DOAS outdoor fan may also be reduced significantly and thereby reduce power consumption as well.

Table 3 also illustrates the correspondence between the power consumption of the steady-state (SS) and (DY) model outputs for the same sets of baseline and optimized inputs. On average, the dynamic models predict 8.9% higher power consumption for the system than the steady-state models; the existence of this discrepancy between the model types is not surprising because of the different assumptions used in the construction of each model. In light of this, however, it is interesting that both the steady-state and dynamic models report fairly similar percentage gains in energy efficiency. This indicates both that the optimized inputs do represent an improved operating condition for the plant, and that using the optimized setpoints obtained from the steady-state models for the dynamic model will represent an improvement over the baseline setpoints for the dynamic model, though the steady-state models will not predict the precise difference in power consumption.

A comparison of the CPU time required to run these simulations supports the use of steady-state models for setpoint optimization. While one run of the steady-state model takes between 10-20 seconds depending on the particular driving conditions, this is a factor of 50-100x faster than is required for the dynamic simulations. These faster simulations have a significant effect on the optimization time; the 16 iterations for the steady-state optimization in Case 1 take 453 seconds, the 13 iterations for the optimization in Case 2 take 475 seconds, and the 11 iterations for Case 3 take 325 seconds, demonstrating that optimized setpoints can be identified for the complex integrated system in a reasonable period of time.

In summary, these results suggest that the use of physical models for setpoint optimization of heterogeneous integrated HVAC can provide significant energy savings for the overall system. The selection of the proper fan speeds is particularly important because these variables are only loosely coupled to the refrigerant-side system dynamics, while as the compressor speeds and valve positions are tightly coupled to performance variables and cannot be independently chosen. This use of physical models is also important because it allows for the calculation and analysis of these setpoint maps at design time, rather than after installation.

Control architecture design

The design of the feedback control loops for the integrated system is non-trivial because of significant dynamic interaction between the DOAS and VRF

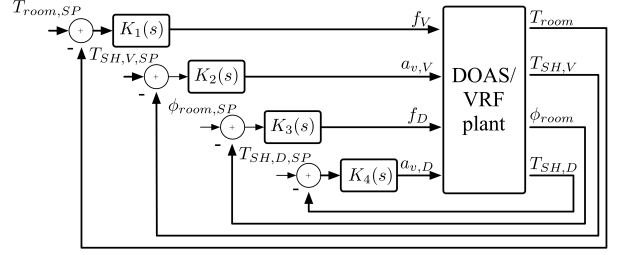


Figure 6: Block diagram of decentralized PI control architecture.

systems. We desire to control the four dimensional vector of measured outputs

$$y = [T_{room}, T_{SH,V}, \phi_{room}, T_{SH,D}]^T,$$

where $T_{SH,V}$ and $T_{SH,D}$ are the evaporator superheats, using the four dimensional vector of inputs

$$u = [f_V, a_{v,V}, f_D, a_{v,D}]^T,$$

where $a_{v,V}$ and $a_{v,D}$ are the positions of the VRF and DOAS linear expansion valves, respectively. The decentralized architecture shown in Figure 6 is preferred, in which each controlled variable y_i is paired to a single actuator u_j , as this structure simplifies the design and commissioning of the control system.

While the obvious pairing of inputs to outputs involves controlling T_{room} using f_V , ϕ_{room} using f_D , and the two superheats using the two LEVs, care must be taken in such a design because of the significant dynamic interaction among the variables. These interactions can be seen in Figure 7, which shows the open loop step responses from the two compressor speeds to T_{room} and ϕ_{room} .

Careful study of Figure 7 reveals two causes of concern. First, the transfer functions from f_D to both relative humidity outputs (lower portion of the figure) show a significant non-minimum phase response, where the offending right-half plane zero has a frequency that is near the desired closed-loop bandwidth. This effect is related to fundamental psychrometric behavior: the rapid drop in room temperature related to the step in compressor frequency results in a temporary increase in the *relative* humidity, followed by a gradual decrease as water is removed from the air on a slower time scale. This behavior will cause closed-loop instability for sufficiently high gains in the DOAS compressor feedback loop.

The second cause for concern is the large gain between f_D and T_{room} (upper right plot of Figure 7) which at steady-state is about three times larger than the gain from f_V . This can also lead to closed-loop instability if the feedback gains are too large because the product of the off-diagonal transfer functions appears as a term in the closed loop transfer functions.

In light of these considerations, we design a PI controller

$$K_j(s) = \frac{k_{pj}s + k_{ij}}{s}$$

	Case 1				Case 2				Case 3			
Parameter	SS _{base}	SS _{opt}	DY _{base}	DY _{opt}	SS _{base}	SS _{opt}	DY _{base}	DY _{opt}	SS _{base}	SS _{opt}	DY _{base}	DY _{opt}
T_{amb} (°C)			35				40				35	
ϕ_{amb} (%)			80				70				80	
Q_{sens} (kW)			18				18				19.2	
Q_{lat} (kW)			7				7				8.2	
Occupants			50				50				70	
f_D (Hz)	36.1	18.6	47.2	24.9	31.9	16.3	40.4	22.2	35.4	25.3	46.6	33.9
f_V (Hz)	54.0	54.1	55.0	55.2	80.3	68.1	89.3	70.7	61.6	62.7	61.9	62.7
$\dot{V}_{OA,D}$ (CFM)	6000	3596	6000	3596	6000	3949	6000	3949	6000	4640	6000	4640
$\dot{V}_{OA,V}$ (CFM)	6000	5143	6000	5143	6000	5998	6000	5998	6000	5996	6000	5996
\dot{V}_{sup} (CFM)	1600	850	1600	850	1600	850	1600	850	1600	1190	1600	1190
\dot{W}_t (kW)	14.30	11.17	15.60	11.90	19.85	14.31	23.11	15.38	15.33	13.54	16.55	14.38
% Imp.	-	21.9%	-	23.7%	-	27.9%	-	33.4%	-	11.7%	-	13.1%
CPU time (s)	10.1	9.8	1280	1337	9.8	9.3	1137	1265	19.5	12.1	1171	900

Table 3: Results obtained by applying optimized setpoints for three different case studies.

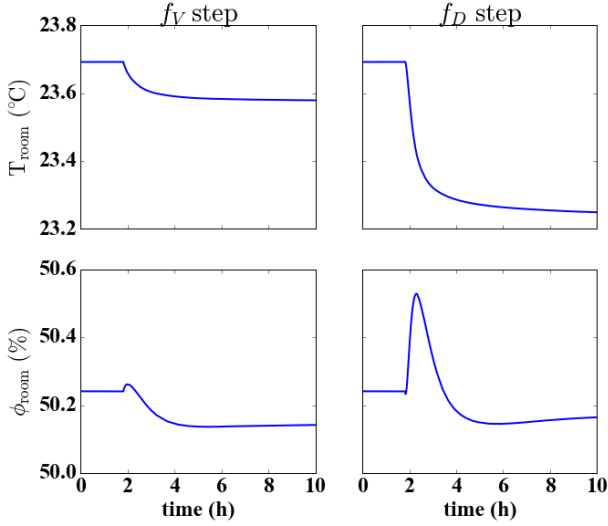


Figure 7: Open loop step responses from VRF compressor speed f_V to T_{room} (top left) and ϕ_{room} (bottom left), and from DOAS compressor speed f_D to T_{room} (bottom left) and ϕ_{room} (bottom right).

for each pairing $j = 1$ to 4 by ignoring the off-diagonal coupling and using only the diagonal terms of the system transfer function to design the PI gains. The closed-loop coupled system can then be analyzed for any loss of stability or performance caused by the off-diagonal terms. Tuning the PI gains to achieve a minimal overshoot and settling time of approximately 2000 s for T_{room} , 4000 s for ϕ_{room} , 200 s for $T_{SH,V}$ and 400 s for $T_{SH,D}$, gives the values in Table 4. We also analyzed the dynamic coupling between the inputs and outputs by using the Nyquist stability criterion (Skogestad and Postelthwaite, 2005) to ensure the stability of the closed-loop system. This analysis confirmed the closed-loop system stability, though the presence of a finite gain margin indicated that the system will lose stability given a sufficient increase in the feedback gains. T_{amb} (°C)

This decentralized controller was implemented on the

Parameter	Value	Parameter	Value
k_{p1} (Hz/°C)	50.0	k_{p3} (Hz/°C)	500.0
k_{i1} (s ⁻¹)	0.05	k_{i3} (s ⁻¹)	0.5
k_{p2} (counts/°C)	0.5	k_{p4} (counts/°C)	0.75
k_{i2} (s ⁻¹)	0.075	k_{i4} (s ⁻¹)	0.03

Table 4: PI controller gains.

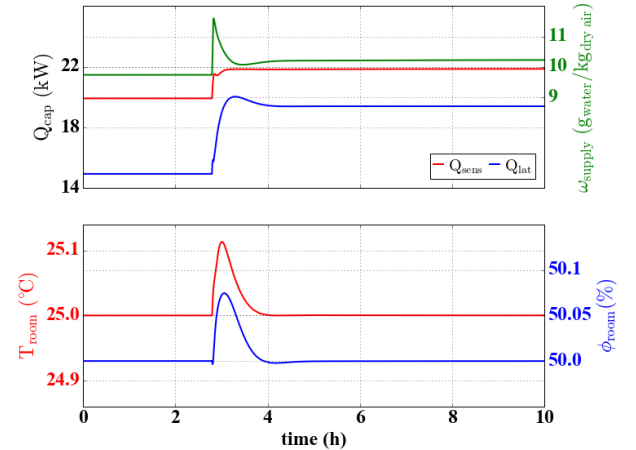


Figure 8: Integrated system behavior in response to an increase in room occupancy from 50 to 70 people.

full nonlinear Modelica model to study the behavior of the closed-loop system. A case study was performed in which we started the system simulation with the conditions listed as Case 1 in Table 3, corresponding to a building occupancy of 50 people, and then increased the supply air flow rate, sensible heat load, and latent heat load to model the effect of 20 additional people entering the building (i.e., Case 3). Each occupant represented a sensible load of 60 W and a latent load of 60 W.

Figure 8 illustrates the effect of this change in room occupancy on the closed-loop integrated system. It is evident from the lower plot in this figure that the control system can effectively manage both the room air temperature and relative humidity; while there is

a small disturbance to both of these variables, the system is able to bring the room conditions back to the setpoint values in approximately 1 hour. The total latent and sensible cooling capacities for both machines, illustrated in the upper plot of Figure 8, also show the ability of the system to respond to the change in the loads.

The importance of such dynamic system analysis can be seen by considering the large increase of the latent machine capacity in response to the occupant disturbance. As is evident from the increased humidity ratio of the supply air, this change in the latent capacity is due to the increase in both the latent load from the occupants and the water vapor entering with the supply air. The impact of such nonintuitive system behavior on the overall building performance can be analyzed with the help of these simulation and optimization approaches, underlining their potential in designing next-generation integrated HVAC systems.

Conclusions

In this paper, we demonstrated a means of using a set of physics-based steady-state and transient models of both space-conditioning systems and building envelopes for simulation, optimization, and control design to achieve high system-level performance. The use of these modeling tools and representations facilitates the rapid exploration of system dynamics to understand the tradeoffs inherent in designing such systems, and can result in significant performance improvements that are readily realized by considering the integrated system as a whole. Future work will include further refinement of these methods as well as experimental validation.

Acknowledgement

The authors would like to thank Andrew Moore and Johnny Glisson at Mitsubishi Electric Cooling & Heating for their expertise and kind assistance in this study.

References

AHRI (2001). Forced-circulation air-cooling and air-heating coils. AHRI 410:2001, Arlington, VA, USA.

ASHRAE (2008). *HVAC Systems and Equipment Handbook*. Atlanta, GA: ASHRAE.

ASHRAE (2016). Ventilation for acceptable indoor air quality. ASHRAE 62.1:2016, Atlanta, GA, USA.

Aute, V. and R. Radermacher (2014). Standardized polynomials for fast evaluation of refrigerant thermophysical properties. In *International Refrigeration and Air-Conditioning Conference at Purdue*.

Aynur, T. (2010). Variable refrigerant flow systems: A review. *Energy and Buildings* 42, 1106–1112.

Fletcher, R. and C. Reeves (1964). Function minimization by conjugate gradients. *Computer Journal* 7, 149–154.

Kim, W., S. Jeon, and Y. Kim (2016). Model-based multi-objective optimal control of a VRF combined system with DOAS using genetic algorithm under heating conditions. *Energy* 107, 196–204.

Laughman, C., H. Qiao, V. Aute, and R. Radermacher (2015). A comparison of transient heat pump cycle models using alternative flow descriptions. *Science and Technology for the Built Environment* 21(5), 666–680.

Modelica Association (2014). Modelica specification, Version 3.3r1.

Mumma, S. and K. Shank (2001). Achieving dry outside air in an energy-efficient manner. *ASHRAE Transactions* 107(1).

Patankar, S. (1980). *Numerical Heat Transfer and Fluid Flow*. Hemisphere Publishing Co.

Qiao, H. and C. Laughman (2016). Modeling of finned-tube heat exchangers: a novel approach to the analysis of heat and mass transfer under cooling and dehumidifying conditions. In *International Refrigeration and Air Conditioning Conference at Purdue*, Number 2298.

Rane, M., D. Vedartham, and N. Bastakoti (2016). Design integration of dedicated outdoor air system with variable refrigerant flow system. In *16th International Refrigeration and Air Conditioning Conference at Purdue*, Number 2439.

Skogestad, S. and I. Postlethwaite (2005). *Multivariable Feedback Control: Analysis and Design*. Wiley.

Stephan, P. (Ed.) (2010). *VDI Heat Atlas*. Springer-Verlag.

Wetter, M., M. Bonvini, and T. Noudui (2016). Equation-based languages – a new paradigm for building energy modeling, simulation, and optimization. *Energy and Buildings* 117, 290–300.

Wetter, M., W. Zuo, T. Noudui, and X. Pang (2014). Modelica buildings library. *Journal of Building Performance Simulation* 7(4), 253–270.

Winkler, J., V. Aute, and R. Radermacher (2008). Comprehensive investigation of numerical methods in simulating a steady-state vapor compression system. *International Journal of Refrigeration* 31, 930–942.

Zhu, Y., X. Jin, Z. Du, and X. Fang (2015). Online optimal control of variable refrigerant flow and variable air volume combined air conditioning system for energy saving. *Applied Thermal Engineering* 80, 87–96.